Supplementary Information

Co(II) Complex-Promoted PVDF β-Phase Crystallization: Innovations in Pressure Sensing and Energy Harvesting

Bapan Jana,[a] Shewli Pratihar,[b] Rajashi Haldar,[a] Akash M Chandran,[b] Dipanti Borah,[a] Prasanna Kumar S Mural,*[b] Maheswaran Shanmugam*[a]

[a]Department of Chemistry, Indian Institute of Technology Bombay Powai,
Mumbai 400076, Maharashtra (India)
E-mail: eswar@chem.iitb.ac.in (MS)

[b]Department of MEMS, Indian Institute of Technology Bombay Powai,
Mumbai 400076, Maharashtra (India)
E-mail: prasannamural@iitb.ac.in (PM)

Experimental section:

Materials and Methods: All of the chemical reagents in the synthesis were of reagent grade and used without further purification.

Single crystal X-ray diffraction measurement: The single-crystal diffraction data of the complex was collected on a Bruker diffractometer with Mo Kα radiation (λ = 0.71073 Å). Data reduction and the unit cell parameters were determined by using CrysAlisPro 1.171.38.43. With the help of Olex2 software with the SHELXL program, crystal data was solved by direct method and refined by the least square procedure. All non-hydrogen atoms were refined anisotropically and the positions of all hydrogen atoms were generated geometrically. The data collection and structure refinement of these crystals are summarized in Table S1. **Powder X-ray diffraction (PXRD):** Powder XRD measurements were carried out in a Rigaku D/tex Ultra 250 instrument, using Cu K_β filter with a scan speed of 5° /min at room temperature and at variable temperatures. Diffraction patterns were collected in the 2θ range of 5°-50° with a step size of 0.01°. **Hirshfeld surface analysis:** The Hirshfeld surface mapping of all the non-covalent molecular interactions of complex Co-Bpy was done using the Crystal Explorer 3.1 program. The single-crystal X-ray crystallographic information file (CIF) was utilized to visualize all the different type of interactions which are present on the Hirshfeld surface. These interactions were obtained as 3D color mapping images such as normalized contact distance (dnorm), shape index and curvedness. The diverse surface colour mappings were generated on the Hirshfeld surface by various colour coding based on strong (red), medium (blue) and weak (white) interactions. **Thermal analyses**: Differential scanning calorimetry (DSC) was done using a Rigaku DSC Vesta instrument by heating and cooling crystalline samples with a rate of 5 K min^{-1} in aluminium crucibles at nitrogen atmosphere. Thermogravimetric analyses (TGA) were carried out on a Rigaku TGMS-ThemoMass Photo instrument by heating crystalline samples with a rate of 5 K/min under nitrogen atmosphere. **Dielectric and ferroelectric measurement:** Complex dielectric permittivity was measured with Keysight Impedance Analyzer E4990A system, where two parallel plate capacitor geometry is considered. Silver conductive paste deposited on both sides of the pressed pellets of the sample were used as top and bottom electrodes. Ferroelectric measurements were also performed on pressed pellets using a Radiant Precision Multiferroic II ferroelectric loop tracer with Model EEL 1102.05.2 high voltage amplifier of Electrical Energy Limited. The pressed pellet (dia ~ 10 mm, thickness ~ 0.65 mm) with silver top and bottom electrodes (diameter ~ 5.2 mm area ~ 22.05 mm^2) is used to harvest thermal energy harvesting.

PFM measurement: Local topography, piezoelectric properties and ferroelectric switching were studied on a pressed pellet by scanning probe microscopy (SPM) technique using piezo-response force microscopy (PFM) in DART (Dual AC Resonance Tracking) mode, in a MFP-3D BIO instrument (Asylum Research) using an SCM-PIT-V2 probe. The amplitude and phase images were recorded by applying fixed ac voltage and the typical butterfly loops and phase loops were recorded by applying different DC biases to tip with the AC voltage.

By the definition of the converse piezoelectric effect, the piezoelectric coefficient (d_{33}) magnitude can be calculated from the equation, $d_{33} = \Delta z/V$; where Δz is the displacement of the tip caused by the deformation of ferroelectric samples under applied electric field and V is the applied voltage. Δz can be calculated from the slope of the linear part of the amplitude vs. voltage curve (butterfly loop) (Jalalian et al., *Appl. Phys. Lett.* 2014, **104**, 103112).

Synthetic procedure for $[Co(bpy)_3](PF_6)_2$ (Co-bpy):

Complex Co-bpy was synthesized as per the literature work reported elsewhere.[S1a] Yield of Co-bpy: 0.56 g (68.5%). Elemental composition of Co-bpy Calc. (%): C, 49.19; H, 3.30; N, 11.46. Found (%): C, 49.16; H, 3.32; N, 11.40.

Scheme S1: Synthetic scheme for the preparation of the complex Co-bpy.

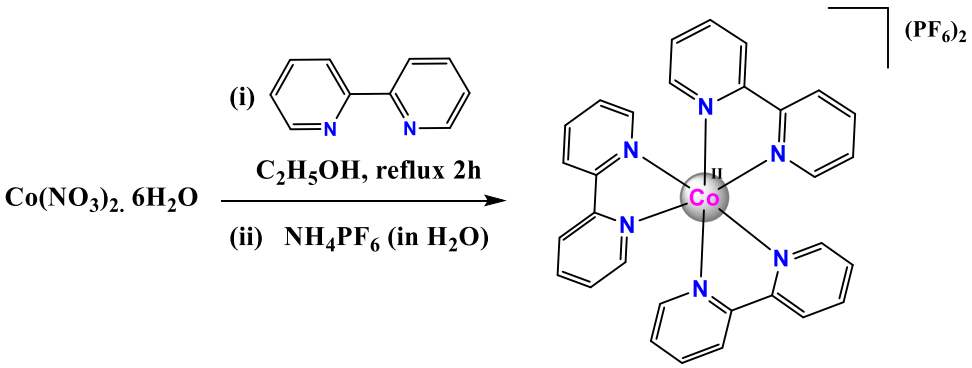

Table S1: Crystallographic parameters for complex Co-bpy.

Parameter	**(150K)**	**(300K)**
Empirical formula	$C_{30}H_{24}CoF_{12}N_6P_2$	$C_{30}H_{24}CoF_{12}N_6P_2$
Formula weight	817.24	817.24
Crystal system	hexagonal	hexagonal
Space group	$P3_1$	$P3_1$
a/Å	10.3401(3)	10.4666(3)
b/Å	10.3401(3)	10.4666(3)
c/Å	26.1342(7)	26.4982(9)
α/°	90	90
β/°	90	90
γ/°	120	120
Volume/$Å^3$	2419.85(15)	2513.96(17)
Z	3	3
$\rho_{calc}g/cm^3$	1.683	1.573
μ/mm^{-1}	0.735	0.705
F(000)	1233.0	1162.0
Crystal size/mm^3	0.28 × 0.22 × 0.18	0.25 × 0.09 × 0.085
Temperature/K	150	300
Radiation	Mo Kα	MoKα
2θ range for data collection/°	4.548 to 49.956	4.494 to 66.042
λ (Å)	(λ = 0.71073)	(λ = 0.71073)
Reflections collected	31452	44411
Independent reflections	5691	10867
Goodness-of-fit on F^2	1.116	0.989
R_1	0.0883	0.0750
wR_2	0.1949	0.1782

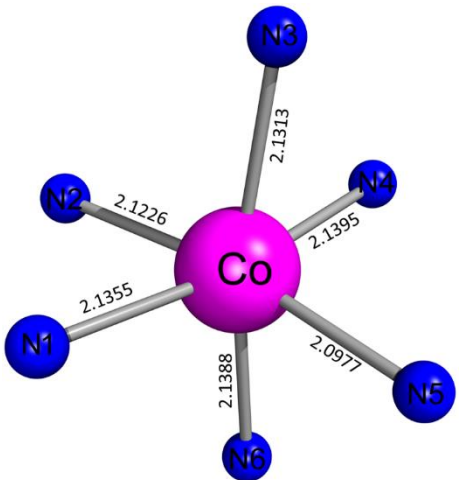

Fig. S1. Selected bond lengths (in Å) of Co-bpy.

Table S2: Selected bond angles for complex Co-bpy**.**

Bond Angle	**Value(°)**
∠N2-Co1-N4	170.2(5)
∠N2-Co1-N5	96.0(5)
∠N2-Co1-N1	79.0(5)
∠N2-Co1-N6	93.2(4)
∠N2-Co1-N3	93.9(5)
∠N4-Co1-N5	90.4(5)
∠N4-Co1-N1	96.1(5)
∠N4-Co1-N6	95.4(5)
∠N4-Co1-N3	77.9(5)
∠N5-Co1-N1	167.7(5)
∠N5-Co1-N6	77.0(5)
∠N5-Co1-N3	96.9(5)
∠N6-Co1-N1	91.9(5)
∠N3-Co1-N1	94.7(5)
∠N3-Co1-N6	171.1(5)

Table S3: Atoms involved in intermolecular hydrogen bonding and its corresponding bond distances and bond angles in complex Co-bpy.

H-Bond Donor (D)-Acceptor(A)	**D...A (Å)**	**∠DHA (°)**
C32-H32...F23_$1	3.08(2)	136
C44-H44...F11_$2	3.44(2)	115.3
C44-H44...F12_$2	3.14(2)	141.8
C51-H51...N3	3.323(19)	118.6
C22-H22...F11_$3	3.166(17)	118.2
C45-H45...F11_$2	3.258(18)	136.8
C45-H45...F16_$2	3.427(19)	130.5
C45-H45...N6	3.33(2)	118
C12-H12...F24	3.29(2)	114.9
C53-H53...F22_$4	3.50(2)	130.2
C23-H23...F11_$3	3.110(18)	123.8
C13-H13...F13_$5	3.222(19)	124.4
C13-H13...F15_$5	3.170(19)	127.9
C31-H31...N2	3.26(2)	115.6
C31-H31...F23_$1	3.33(2)	113.6
C24-H24...F16	3.144(17)	117.5
C25-H25...F12	3.485(19)	144.2
C25-H25...N5	3.376(19)	116.4
C11-H11...N4	3.33(2)	117.5
C11-H11...F24	3.35(2)	111.9
C11-H11...F22	3.35(2)	124.1
C43-H43...F25_$6	3.14(2)	113.8
C42-H42...F14_$7	3.119(19)	142
C62-H62...F24_$8	3.42(2)	117.9
C62-H62...F23_$8	3.36(2)	144.9

C34-H34...F14_$7	3.301(19)	120.5
C65-H65...N1	3.21(2)	118.3
C63-H63...F24_$8	3.25(2)	131.7
C52-H52...F24_$4	3.48(2)	161.7
C52-H52...F25_$4	3.47(2)	134.9

$1 = X, Y-1, Z; $2 = X, Y+1, Z; $3 =Y+2, -X+1, Z-0.333; $4 =-Y+1, X-Y, Z+0.333; $5 = Y+2, -X+2, Z-0.333; $6 = -Y+1, X-Y+1, Z+0.333; $7 = X-1, Y, Z; $8 = -Y+2, X+1, Z+0.333.

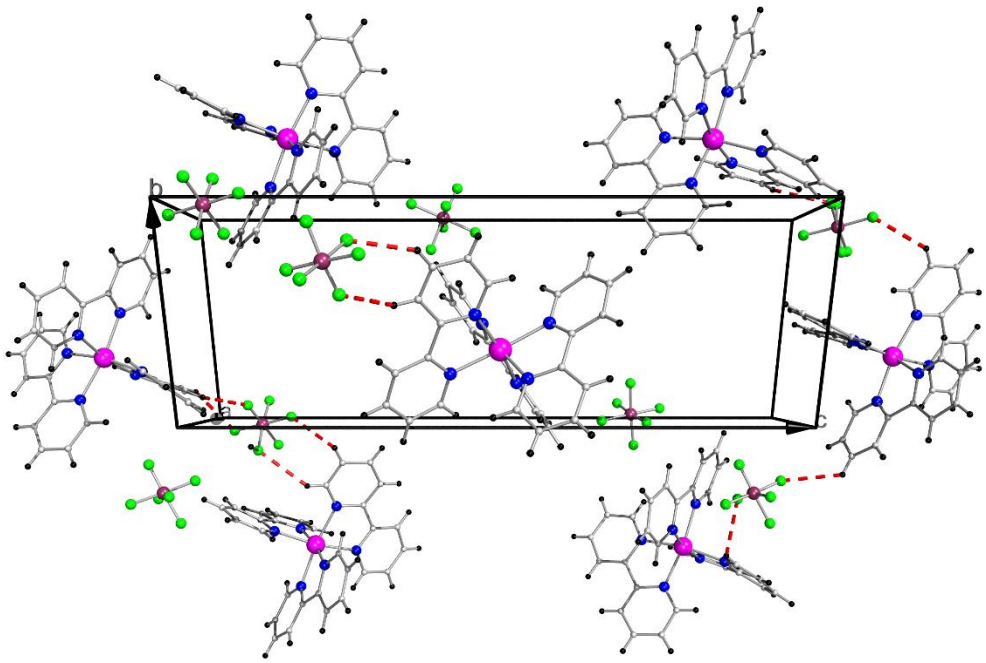

Fig. S2. Packing diagram of Co-bpy. Orange dotted lines represent F…H hydrogen bonding between H atom of C-H bond of Bpy and F atom of PF_6 anion. Colour Code: Cobalt: purple; Carbon: dark grey; Nitrogen: blue; Oxygen: Red; Fluorine: green; Hydrogen: black.

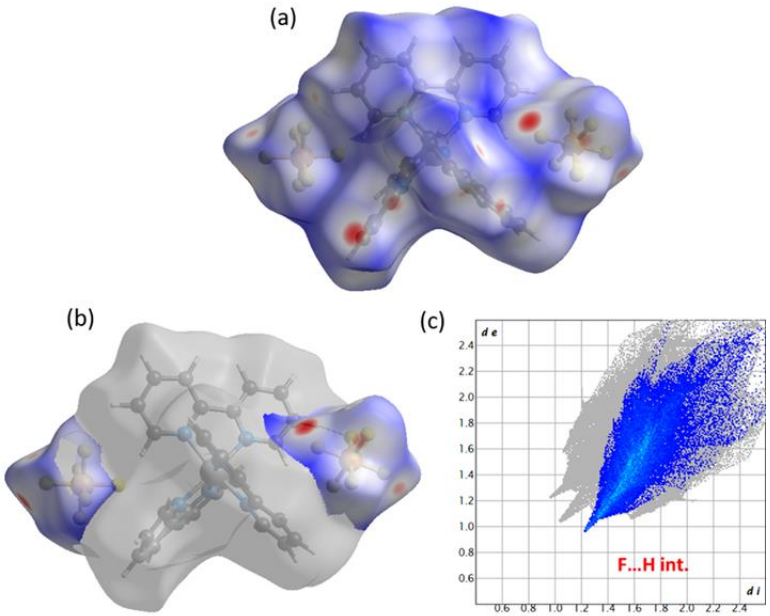

Fig. S3. (a) Hirshfeld surface view of Co-bpy, (b) Hirshfeld surface view of intramolecular H-bonding interaction, (c) two-dimensional fingerprint plot of F···H (24.8%) interaction.

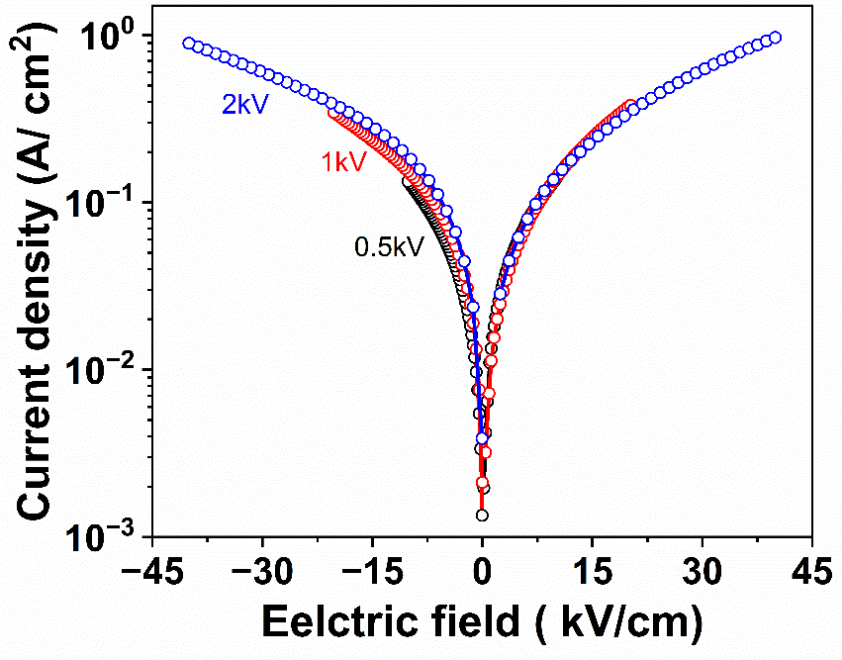

Fig. S4. The leakage current density (J) Vs. Electric field (E) under different voltage for a Co-bpy complex with thickness of 0.51 mm. at room temperature.

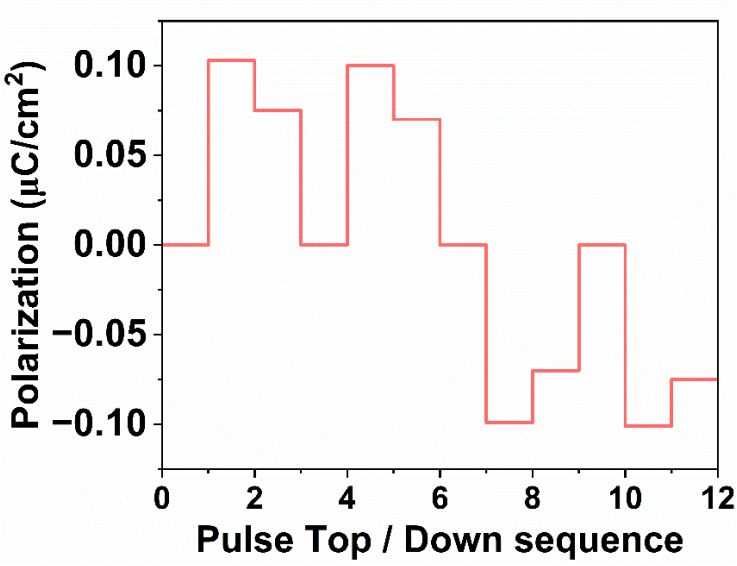

Fig. S5. PUND sequence (Positive up and negative down) with a Pulse Width = 10 ms and Pulse Delay = 100 ms, at 5Hz frequency for Co-bpy complex to conform true ferroelectric switching behaviour.

Device fabrication: Appropriate quantities of crystals of complex Co-Bpy were added to a 10 weight percent (wt%) solution of poly(vinylidene-Fluoride) (PVDF) in N,N-dimethylformamide (DMF), followed by stirring at 70 °C temperature, to prepare 3, 5, 7, 10, and 15 wt % (w/V) composite solutions. The solutions were then drop casted on glass substrate and dried up at ~ 65 °C for 5 h, to prepare the flexible composite films, which were then used for device fabrication.

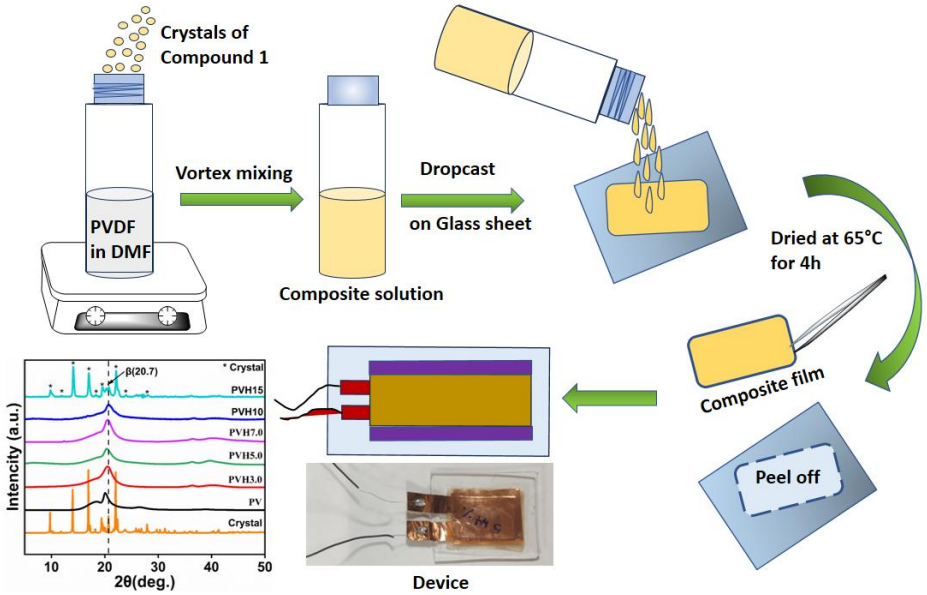

Scheme S2: Schematics of the composite film preparation.

The low-coat and flexible neat and composite PENGs were fabricated by using copper adhesive tapes as the top and bottom electrodes on either side of the films of dimension (2 cm × 2 cm). Wires were then connected to each electrode for electrical measurements. The device was encapsulated within polydimethylsiloxane (PDMS) to protect it from any external damage, using Dow Corning Sylgard 184 elastomer and curing agent in the ratio (10:1) followed by drying at 60°C for 40 mins.

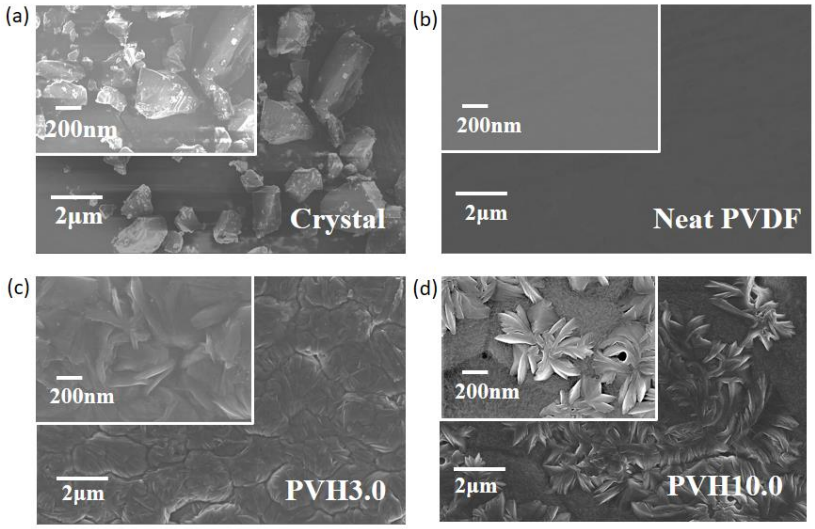

Fig. S6. Field emission scanning electron microscopy (FE-SEM) images of (a) only crystal, (b) neat PVDF film (c) PVH3.0 i.e. composite film made at 3 wt % and (d) PVH10.0 i.e. composite film made at 10 wt %.

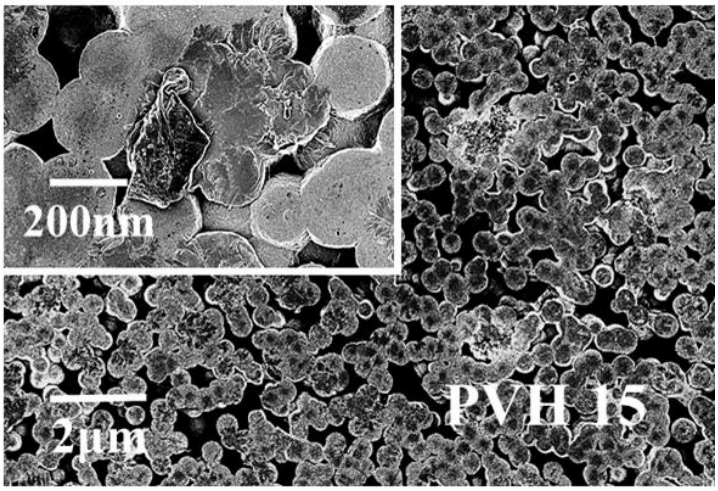

Fig. S7. Field Emission Scanning Electron Microscopy (FE-SEM) images of PVH 15 agglomerated composite films at scales of 2 µm and 200 nm.

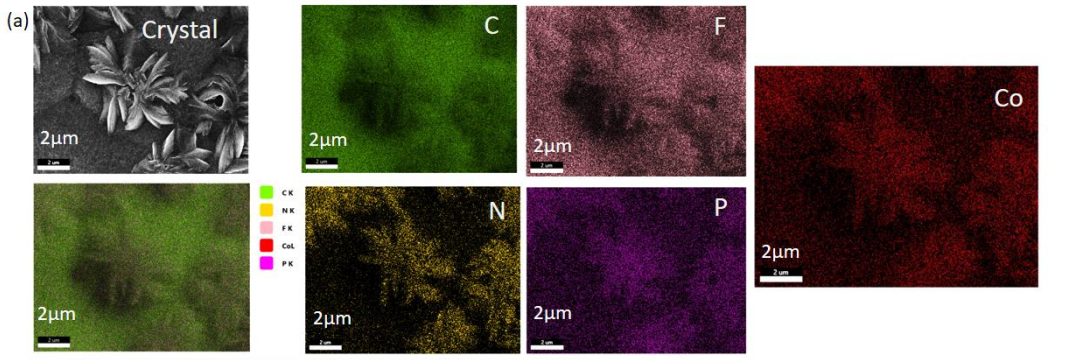

Element	Weight %	Atomic %
C K	69.02	77.34
N K	7.04	6.76
F K	20.94	14.83
P K	1.82	0.79
Co K	1.18	0.27

Fig. S8. a) SEM-EDS mapping images of PVH10.0 composite film, b) EDS spectra of PVH10.0 and corresponding atomic percentage of different elements.

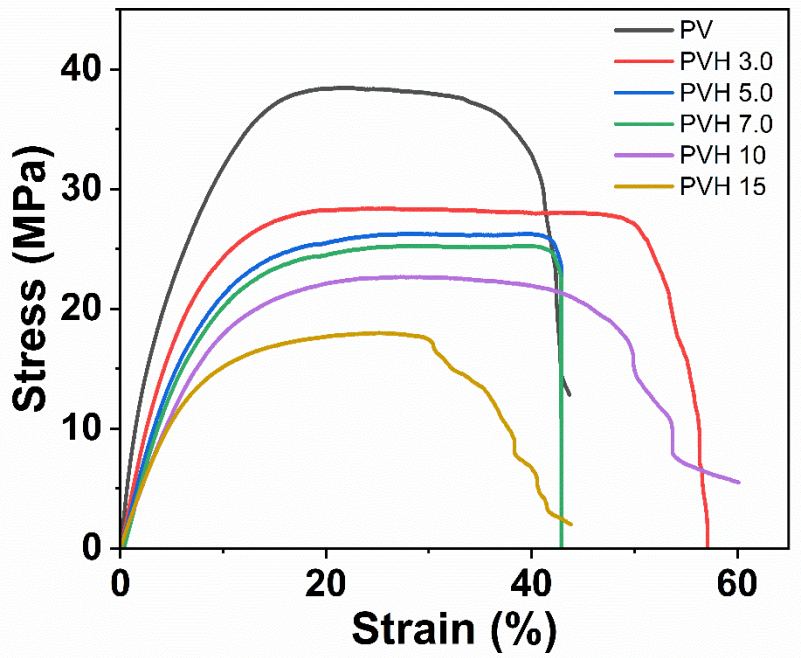

Fig. S9. The stress-strain profile of PVDF and PVDF/Co-bpy composite films.

Table S4.Tensile properties performed on the PVDF and PVDF/Co-bpy composite films.

Sample	Tensile Strength (MPa)	Elongation at break (%)
PV	35.53	37.78
PVH 3.0	27.39	49.26
PVH 5.0	25.68	42.19
PVH 7.0	24.97	41.63
PVH 10	20.59	44.57
PVH 15	17.45	30.06

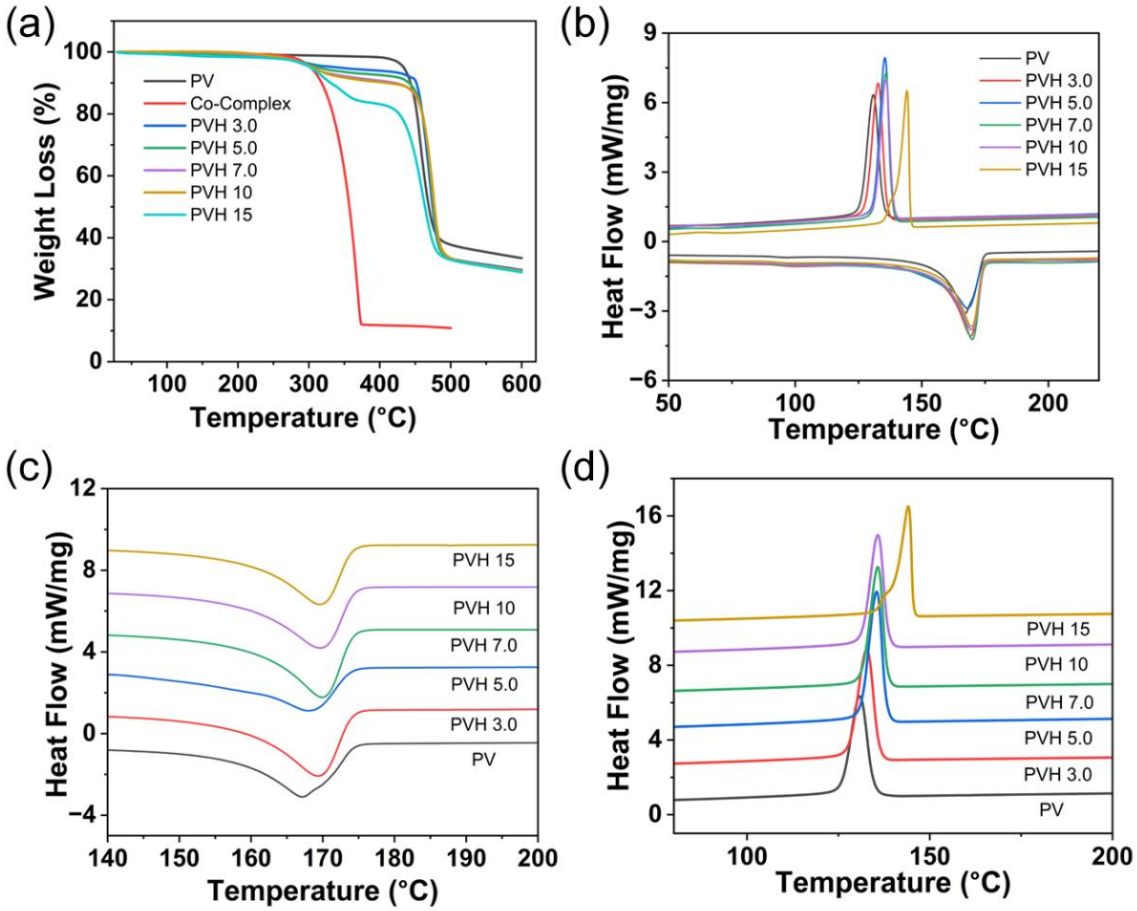

Fig. S10. (a) TGA (b) DSC heating and cooling (c) DSC heating (d) DSC Cooling curve of PVDF and PVDF/Co-bpy.

Table S5. DSC results for PVDF and PVDF/Co-bpy composite films.

Sample	T_m (°C)	T_c (°C)
PV	167.1	130.83
PVH 3.0	169.35	132.55
PVH 5.0	169.42	135.23

PVH 7.0	169.90	135.54
PVH 10	170.2	135.86
PVH 15	169.82	143.74

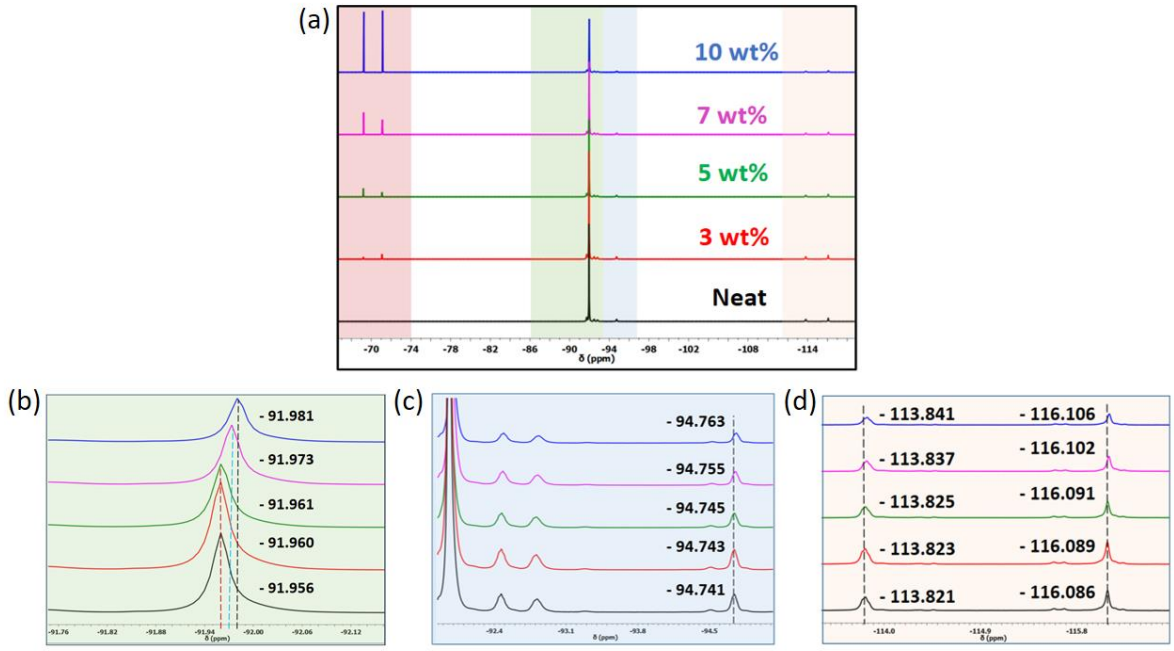

Fig. S11. Solution-state NMR (^{19}F NMR) spectra of the composites at different concentrations of Co-bpy.

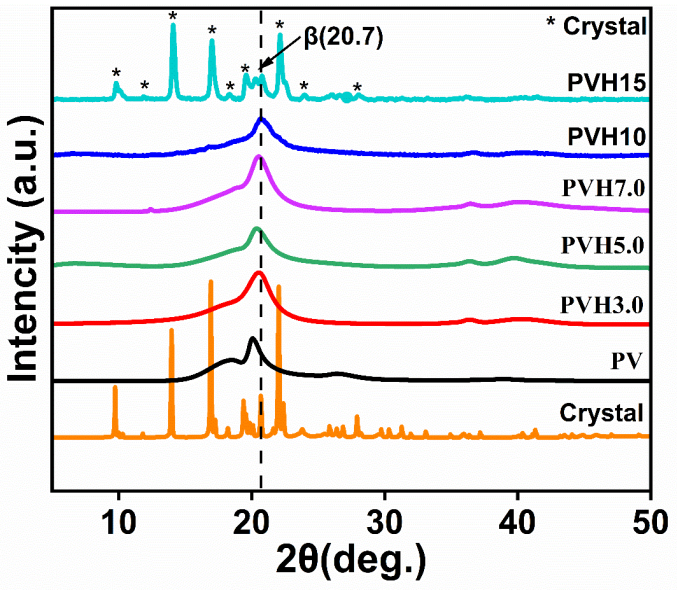

Fig. S12. PXRD pattern of PVDF and all nanocomposite films (5º to 50º)

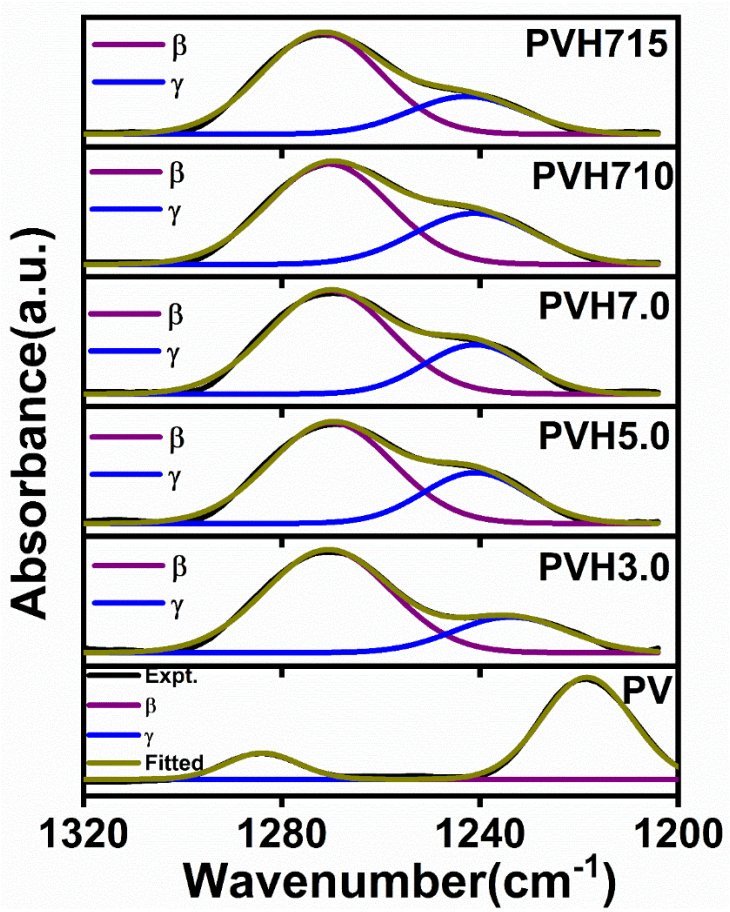

Fig. S13. The deconvoluted FTIR spectra (range within 1320-1200 cm^{-1}) of PVDF and all the nanocomposites.

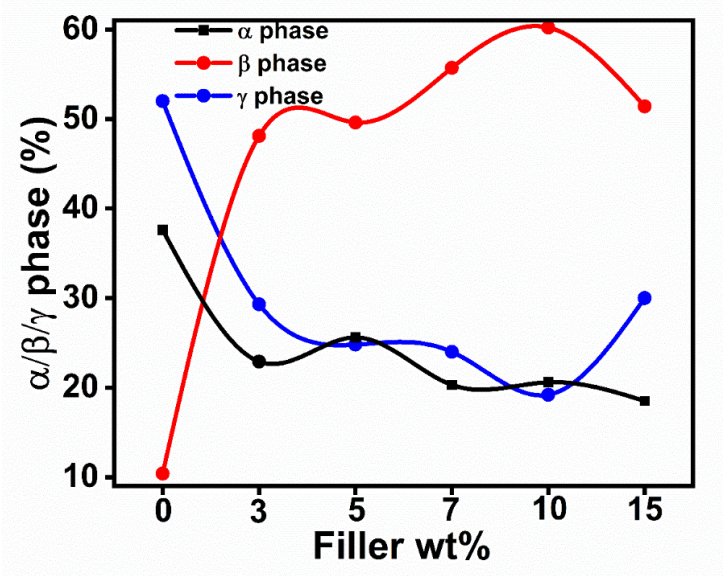

Fig. S14. Variation of α, β and γ phase percentage with crystal wt. % in the PVDF matrix.

Table S6: Individual amount of polar phase calculation for PVDF and all nanocomposite films.

Sample Name	Polar phase Fraction (F_{EA} %)	β phase Fraction (F_β %)	γ phase Fraction (F_γ %)	α phase Fraction (F_α %)
PVDF	48	10.4	37.6	52
PVH3.0	70.7	48.1	22.9	29.3
PVH5.0	75.2	49.6	25.6	24.8
PVH7.0	76	55.7	20.3	24
PVH10	80.8	60.2	20.6	19.2
PVH15	70	51.4	18.5	30

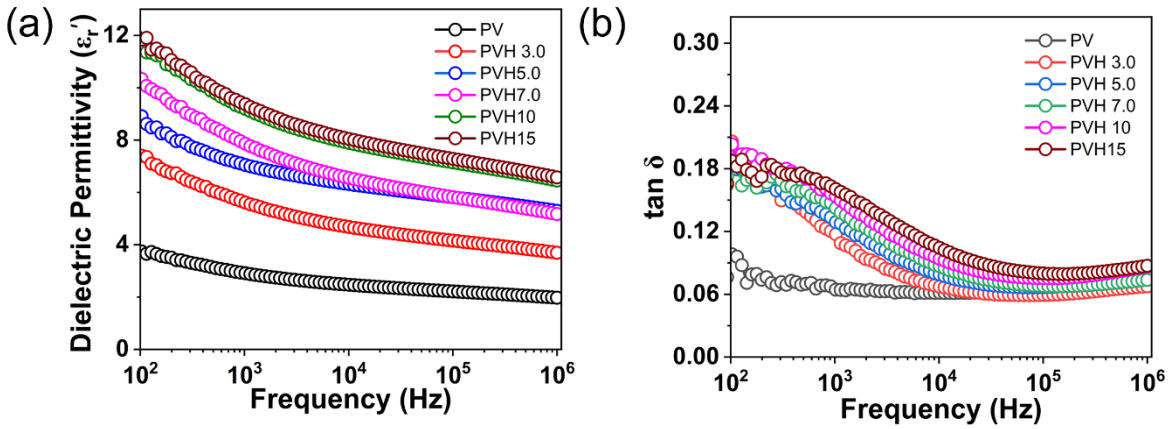

Fig. S15. (a) Dielectric permittivity (b) Dielectric loss (tan δ) of PVDF/Co-bpy composite films at room temperature (10^2 – 10^6 Hz).

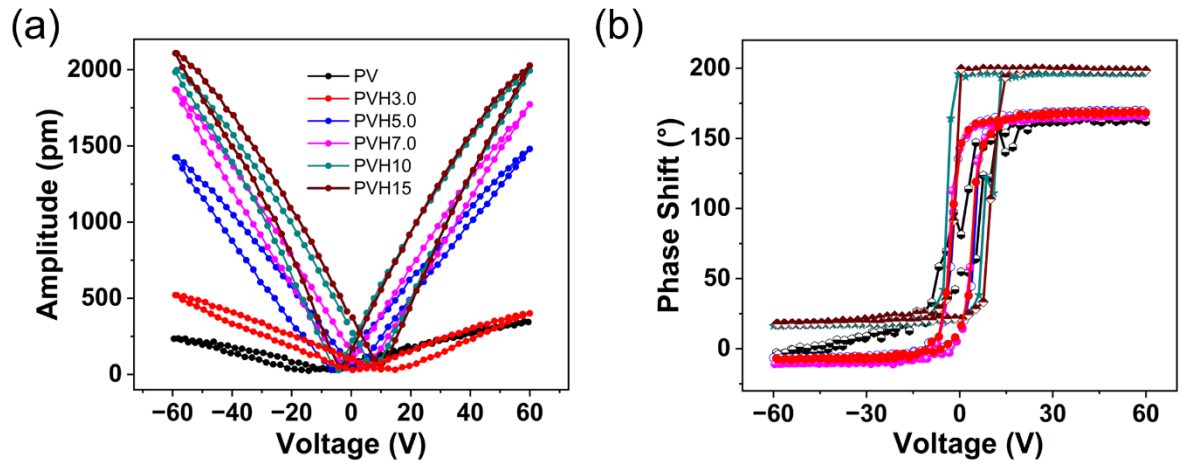

Fig. S16. (a) Amplitude-Voltage butterfly loop, (b) Phase shift-Voltage hysteresis loop.

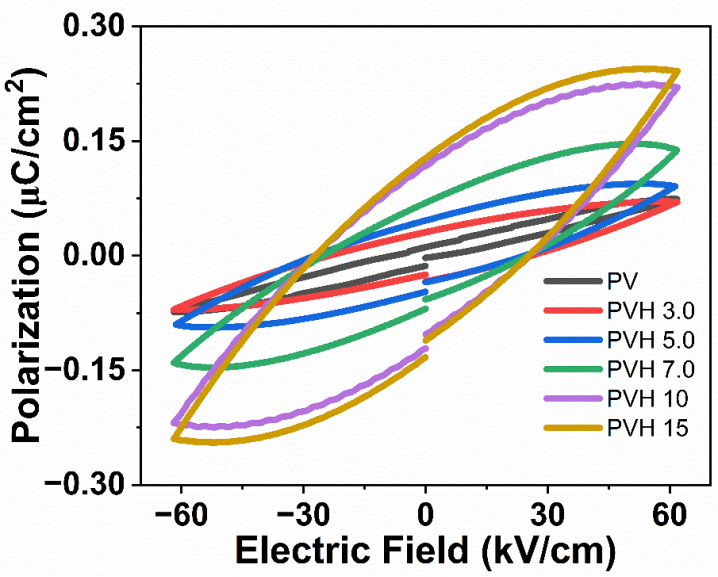

Fig. S17. Polarization (P) vs Electric Field (E) hysteresis loop measured at room temperature in the PVDF/ Co-bpy composite films at 5Hz.

Table S7: Output voltage and current of PVDF and all the nanocomposite system.

Piezoelectric Device	Output Voltage (V)	Output Current (μA)
PVDF	2.9	0.3
PVH3.0	6.2	0.442
PVH5.0	7.45	0.635
PVH7.0	9.6	0.86
PVH10	13.5	1.356
PVH15	8.69	0.83

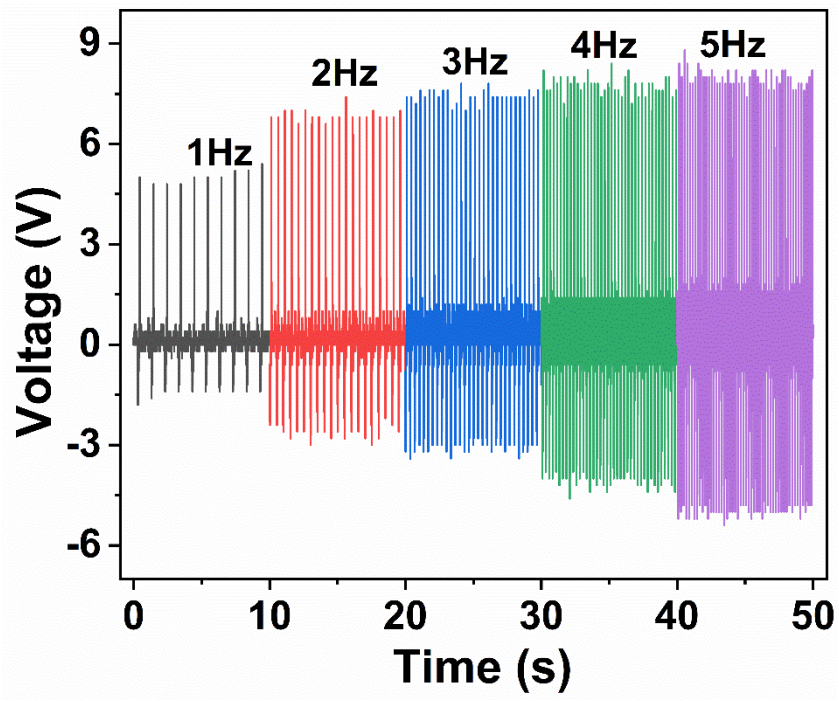

Fig. S18. Voltage *vs* time response of composite film under 1, 2,3,4 and 5 Hz frequency.

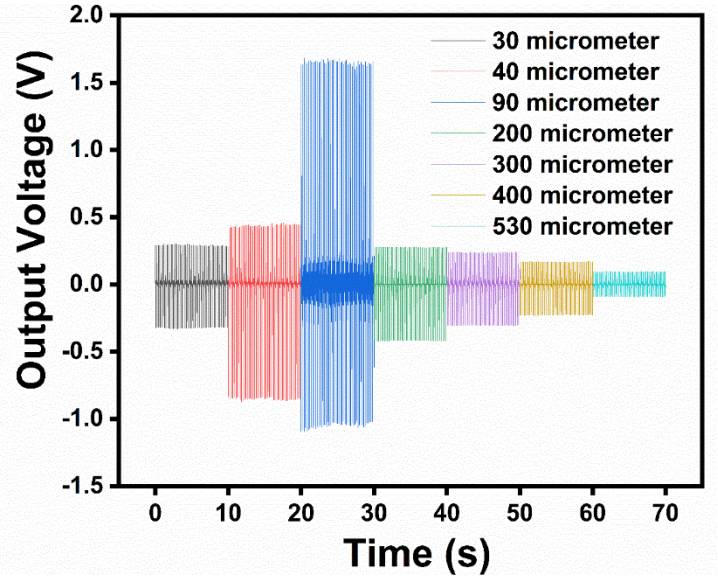

Fig. S19. Output voltage vs thickness variation of PVDF

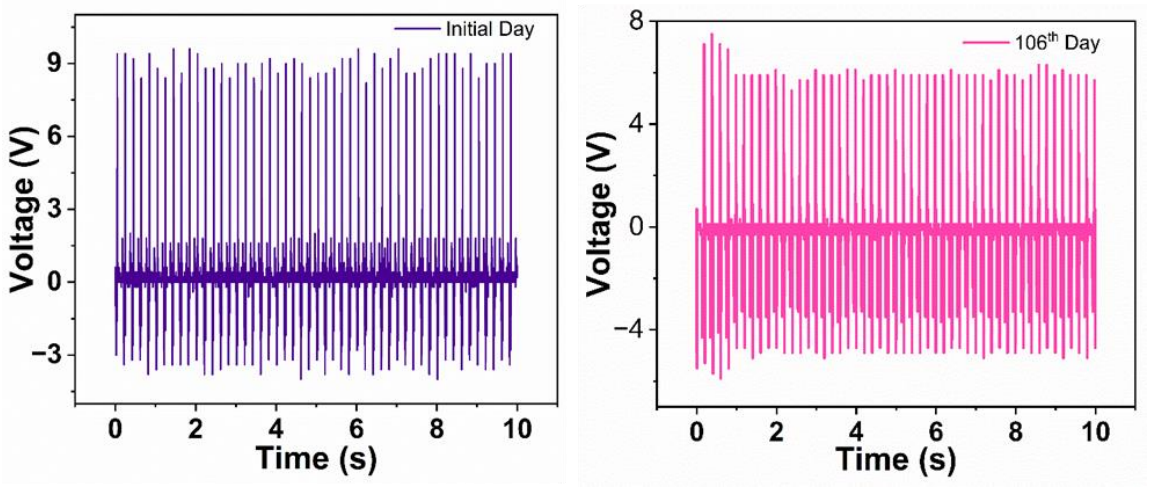

Fig. S20. The durability of PVH10 composite film recorded on the initial day and the 106th day.

Fig. S21. Digital image of LED illumination by the PVH10 PENG.

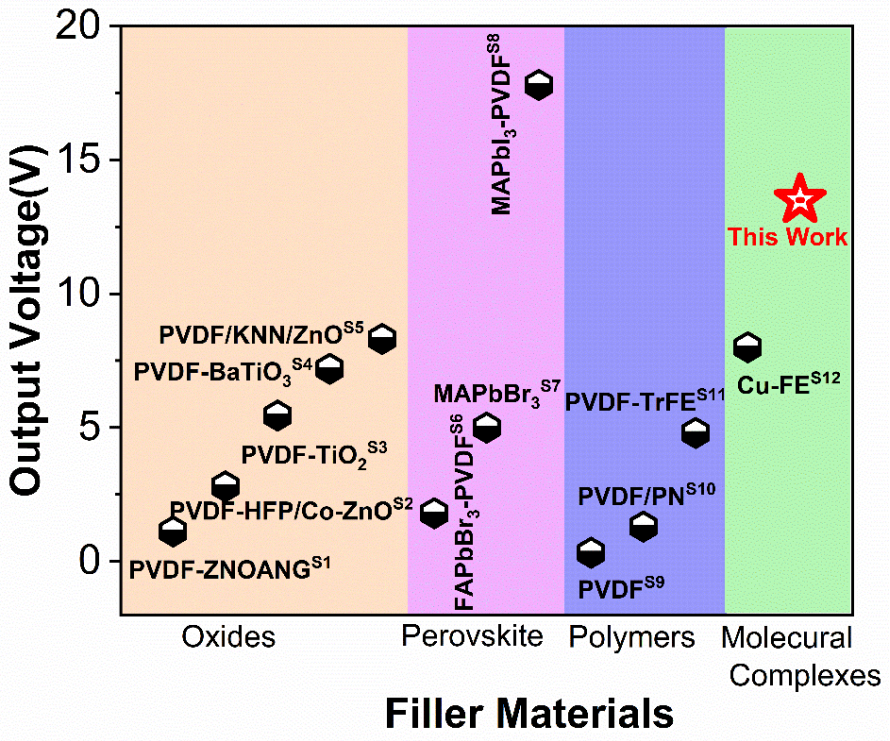

Fig. S22. A comparison of the values of output Voltage obtained from the flexible PENG devices made using Co-bpy and other filler materials incorporated in PVDF reported so far.

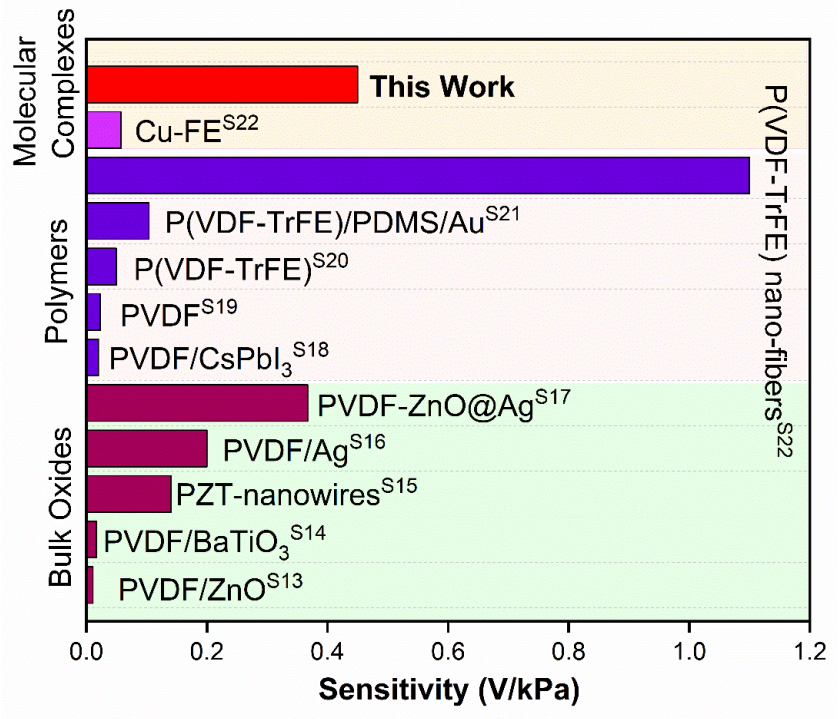

Fig. S23. Comparison of pressure sensing performance of the fabrication PENG devices made using Co-bpy and other filler materials incorporated in PVDF reported so far.

Supporting video

SV1 A video displaying the PVH10 PENG illuminating 2 green LEDs in series connection.

References:

[S1a] P. M. Björemark, J. Jönsson and M. Håkansson, *Chem. Eur. J.*, 2015, **21**, 10630-10633.

[S1] B. Sun, X. Li, R. Zhao, H. Ji, J. Qiu, N. Zhang, D. He and C. Wang, *J. Mater. Sci.*, 2019, **54**, 2754-2762.

[S2] H. Parangusan, D. Ponnamma and M. A. A. Al-Maadeed, *Sci. Rep.*, 2018, **8**, 754.

[S3] N. D. Kulkarni and P. Kumari, *Mater. Res. Bull.*, 2023, **157**, 112039.

[S4] M. Sahu, S. Hajra, K. Lee, P. Deepti, K. Mistewicz and H. J. Kim, *Crystals*, 2021, **11**, 85.

[S5] S. Bairagi and S. W. Ali, *Int. J. Energy Res.*, 2020, **44**, 5545-5563.

[S6] A. Sultana, P. Sadhukhan, M. M. Alam, S. Das, T. R. Middya and D. Mandal, *ACS Appl. Mater. Interfaces*, 2018, **10**, 4121-4130.

[S7] A. Sultana, M. M. Alam, P. Sadhukhan, U. K. Ghorai, S. Das, T. R. Middya and D. Mandal, *Nano Energy*, 2018, **49**, 380-392.

[S8] V. Jella, S. Ippili, J.-H. Eom, J. Choi and S.-G. Yoon, *Nano Energy*, 2018, **53**, 46-56.

[S9] Shafii, C. Energy Harvesting Using PVDF Piezoelectric Nanofabric. University of Toronto, 2014.

[S10] Z. Liu, G. Li, Q. Qin, L. Mi, G. Li, G. Zheng, C. Liu, Q. Li and X. Liu, *Adv. Compos. Hybrid Mater.*, 2021, **4**, 1215-1225.

[S11] N. Bhadwal, R. Ben Mrad and K. Behdinan, *Nanomaterials*, 2023, **13**, 3170.

[S12] R. Haldar, U. Sarkar, A. Kumar, D. Mandal and M. Shanmugam, *Adv. Funct. Mater.*, 2024, **34**, 2407611.

[S13] W. Feng, Y. Chen, W. Wang and D. Yu, *Colloids Surf. A Physicochem. Eng. Asp.*, 2022, **633**, 127890.

[S14] W. Guo, C. Tan, K. Shi, J. Li, X.-X. Wang, B. Sun, X. Huang, Y.-Z. Long and P. Jiang, *Nanoscale*, 2018, **10**, 17751-17760.

[S15] Q.-L. Zhao, G.-P. He, J.-J. Di, W.-L. Song, Z.-L. Hou, P.-P. Tan, D.-W. Wang and M.-S. Cao, *ACS Appl. Mater. Interfaces*, 2017, **9**, 24696-24703.

[S16] M. Lou, I. Abdalla, M. Zhu, J. Yu, Z. Li and B. Ding, *ACS Appl. Mater. Interfaces*, 2020, **12**, 1597-1605.

[S17] Y. Ma, M. Liu, Y. Feng, H. Zheng and Y. Wu, *J. Mater. Res. Technol.*, 2022, **20**, 2689-2704.

[S18] B. Mondal, H. K. Mishra, D. Sengupta, A. Kumar, A. Babu, D. Saini, V. Gupta and D. Mandal, *Langmuir*, 2022, **38**, 12157-12172.

[S19] V. Gupta, A. Babu, S. K. Ghosh, Z. Mallick, H. K. Mishra, D. Saini and D. Mandal, *Appl. Phys. Lett.*, 2021, **119**.

[S20] A. Kumar, D. Saini and D. Mandal, *Appl. Phys. Lett.*, 2022, **120**.

[S21] K. Parida, V. Bhavanasi, V. Kumar, R. Bendi and P. S. Lee, *Nano Res.*, 2017, **10**, 3557-3570.

[S22] R. Haldar, U. Sarkar, A. Kumar, D. Mandal and M. Shanmugam, *Adv. Funct. Mater.*, 2024, **34**, 2407611.